Leaf-Like V_2O_5 Nanosheets Fabricated by a Facile Green Approach as High Energy Cathode Material for Lithium-Ion Batteries

*Yanwei Li, Jinhuan Yao, Evan Uchaker, Jianwen Yang, Yunxia Huang, Ming Zhang, and Guozhong Cao**

Lithium-ion batteries (LIBs) have attracted considerable attention due to their wide applications, such as in portable electronic devices, implantable medical devices, and electric vehicles (EVs).[1] To meet the constantly increasing demands of upcoming electronic devices, new LIBs require substantial improvements in energy capacity, cycling stability, and rate capability of both the cathode and anode materials.[2,3] Among cathode materials for LIBs, orthorhombic vanadium pentoxide (V_2O_5) the most stable form in the vanadium oxide family, has gained great interest due to its high energy density, low cost, abundant sources, and good safety properties.[4–7]

The theoretical capacity of V_2O_5 with two Li intercalations/deintercalations is about 294 mA h g^{-1}, much higher than those of more commonly used cathode materials, making it a very promising cathode material for next-generation LIBs. However, the practical use of V_2O_5 as cathode materials for LIBs has been hampered due to its poor cycling stability, low electronic and ionic conductivity, and slow electrochemical kinetics.[8–10] To overcome these problems, decreasing their particle size to nanoscale level is generally believed to be one of the most effective approaches due to the shorter transport lengths for both electrons and Li ions, larger electrode/electrolyte contact area, and better accommodation of the strain of Li intercalation/deintercalation in nanomaterials.[11,12] The unique performance of nanomaterials lies in their large specific surface and favorable structural properties. 2D nanosheets often possess large exposed surfaces and specific facets, which make them more attractive in energy conversion devices.[13] 2D structures are ideal frameworks for fast Li storage, which requires stability, large active surface area, and short transport path for Li intercalation/deintercalation.[14] There have been many researches on nanostructured V_2O_5 materials for LIBs.[4–7,15–20] However, there are few reports on 2D nanostructured V_2O_5 for LIBs. The only report on 2D nanostructured V_2O_5 was that Zhang's group prepared large-area pure V_2O_5 nanosheets by dissolution-splitting method from their parent bulk cyrstal using ammonium persulfate as intercalated compound.[21] The method is a typical top-down method. The as-prepared product exhibits enhanced lithium storage properties including high reversible capacity, good cycling, and rate performance.

In this communication, we demonstrate a novel and facile green method to prepare 2D leaf-like V_2O_5 nanosheets as illustrated in **Figure 1**. V_2O_5 powders were reacted with H_2O_2 in combination with ultrasonic treatment to generate V_2O_5 gel. Then the V_2O_5 gel was diluted, freeze-dried, and further treated at 450 °C in air to obtain V_2O_5 nanosheets. Used as cathode material for LIBs, this 2D leaf-like V_2O_5 nanosheets exhibits excellent Li storage properties, including high reversible capacity, high rate capability, and good capacity retention upon cycling. The low-cost raw materials (only commercial V_2O_5 powder and H_2O_2 without using any templates) and facile experimental procedures favorably enable the method suitable for large-scale production.

Figure 2 presents the FESEM and TEM images of the V_2O_5 nanosheets annealed at 450 °C for 1 h in air. It can be clearly seen that the prepared V_2O_5 has a large-area 2D leaf-like structure (Figure 2a). The thickness of the V_2O_5 nanosheets is 60 ~ 80 nm (Figure 2b). From the SEM image shown in Figure 2b, one can find that the V_2O_5 nanosheet actually is polycrystalline and consists of small nanorods. The TEM image (Figure 2c) further confirms the 2D sheet structure of the prepared V_2O_5. The high resolution (HR) TEM image (Figure 2d) of the V_2O_5 nanosheet displays clear lattice fringes with a spacing of 0.26 nm and is indexed to the (310) planes of orthogonal V_2O_5 (JCPDS

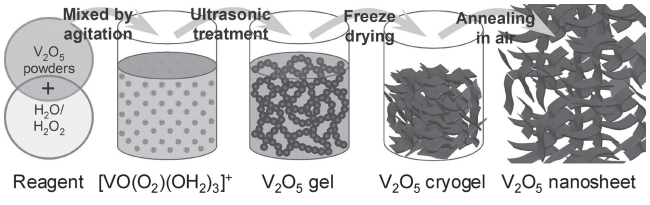

Figure 1. Schematic illustration of the synthesis route of 2D leaf-like V_2O_5 nanosheets in this work.

Prof. Y. Li, E. Uchaker, Prof. Y. Huang, M. Zhang, Prof. G. Cao
Department of Materials Science and Engineering
University of Washington
Seattle, WA, 98195, USA
E-mail: gzcao@u.washington.edu
Prof. Y. Li, J. Yao, J. Yang
Key Laboratory of New Processing Technology for Nonferrous Metals and Materials
Ministry of Education
Guilin University of Technology
Guilin, 541004, PR China
E-mail: lywhit@126.com

DOI: 10.1002/aenm.201300188

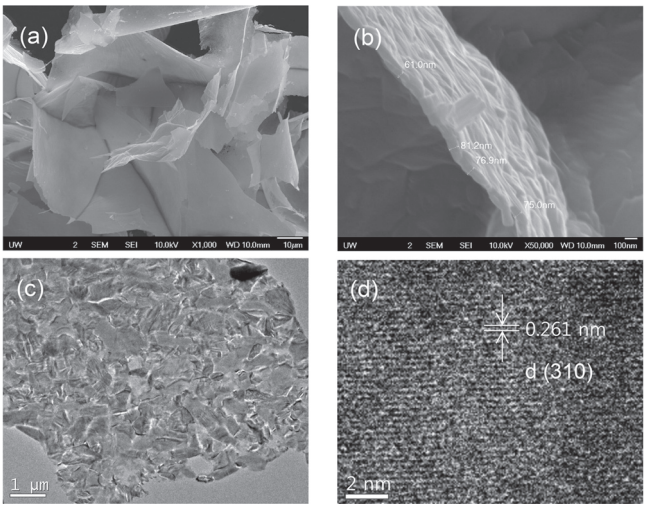

Figure 2. (a) Low- and (b) high-magnification FESEM images of V_2O_5 nanosheet; (c) TEM image of individual V_2O_5 nanosheet; (d) high resolution TEM (HRTEM) image of the selected area in Figure 2c.

card No. 41-1426). The mechanism for the formation of this 2D V_2O_5 nanosheet can be described as follows. During the process of freeze drying, the ribbon-like V_2O_5 fibers intertwines into sheets V_2O_5 during the removal of solvent from the V_2O_5 gel. The freeze-dried V_2O_5 cryogel consists of long nanobelts which are less than 100 nm wide (see Supporting Information, Figure S2). These nanobelts morphology could be related to the formation of hydrous V_2O_5 as previously reported in literature,[22,23] and this is in good agreement with the XRD diffraction results (see Supporting Information, Figure S3). When the V_2O_5 cryogel are annealed in air at 450 °C, the hydrous V_2O_5 nanobelts grow into small nanorods and formed orthorhombic leaf-like V_2O_5 nonosheets.

Figure 3a shows the XRD pattern of the V_2O_5 nanosheets annealed at 450 °C for 1 h in air. All the diffraction peaks can be indexed to an orthorhombic phase V_2O_5 (JCPDS card No. 41-1426) with the lattice parameters of a = 11.488 Å, b = 3.559 Å, c = 4.364 Å, agreeing well with literatures.[5,17,18] No secondary phase is observed. The orthorhombic phase V_2O_5 has a layered structure consisting of V_2O_5 layers stacking along the c-axis (the inset of Figure 3a).[22] Nitrogen adsorption/desorption isotherm measurement was carried out and the results are shown in Figure 3b. The Barrett-Joyner-Halenda (BJH) pore size distribution obtained from the isotherm reveals that the sample contains relatively mesoscale pores. The Brunauer-Emmett-Teller (BET) specific surface area has been estimated to be 28 m^2 g^{-1}.

Figure 4a presents the cyclic voltammetry (CV) profiles of 2D leaf-like V_2O_5 nanosheets electrode for the first two cycles at a scan rate of 0.2 mV s^{-1}. In the first cycle, the three intensive reduction peaks located at 3.30, 3.08, and 2.17V correspond to the phase transitions α/ε, ε/δ, and δ/γ, respectively.[24] Three obvious oxidation peaks appears during the anodic scanning, at 2.57, 3.35, and 3.48 V, respectively. An additional cathodic peak observed in the high potential region (at 3.56 V) can be ascribed to the irreversible phase transition of the γ/γ' system.[25] The symmetrical feature of the CV curve suggests

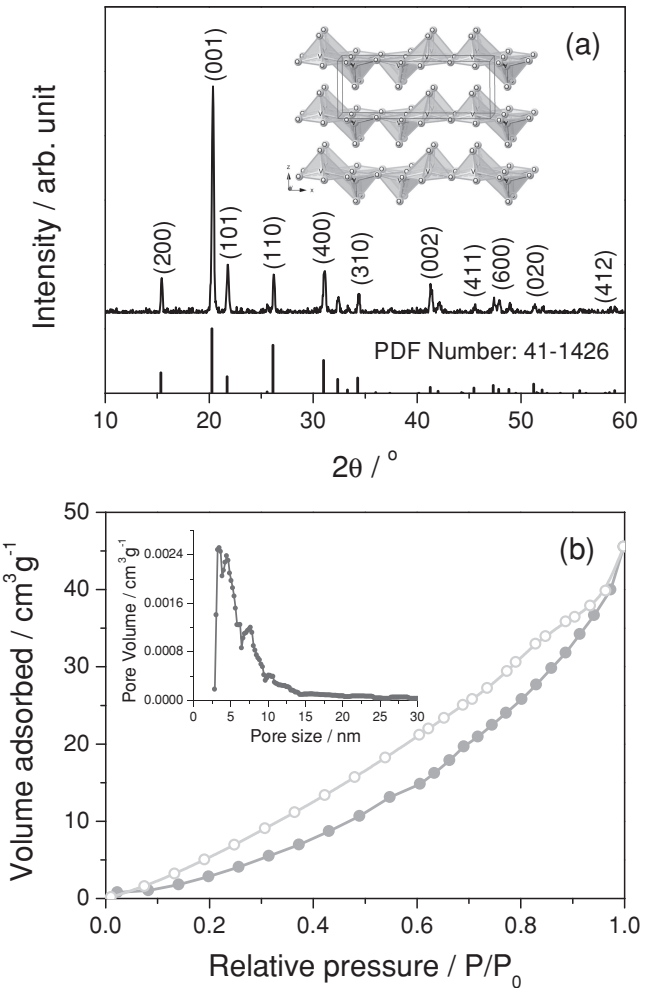

Figure 3. (a) XRD pattern of leaf-like V_2O_5 nanosheets. The vertical lines on the x-axis correspond to the standard XRD reflections of orthorhombic V_2O_5 and the inset shows crystalline structure of layered V_2O_5. (b) N_2 adsorption/desorption isotherm and corresponding BJH pore-size distribution curves (inset) of leaf-like V_2O_5 nanosheets.

a good reversibility of the cycling process. Figure 4b gives the cycling response of 2D leaf-like V_2O_5 nanosheets electrode at various charge/discharge current densities. The discharge capacities measured in the voltage window from 2.0 V to 4.0 V are 303, 273, 251, 219, and 160 mA h g^{-1} at the current densities of 50, 200, 500, 1000, and 2000 mA g^{-1}, respectively. Even at a very high current density of 5000 mA g^{-1}, the 2D leaf-like V_2O_5 nanosheets electrode can still deliver high capacity of 104 mA h g^{-1}. This rate capability is better than those of nanostructured V_2O_5 electrodes reported in literatures (see Supporting Information, Figure S4).[5,26–29] The results from this study show that the 2D leaf-like V_2O_5 nanosheets structure favorably reduces the diffusion length for lithium ions and enables the high rate performance of LIBs. With the charge/discharge current density increasing from 50 to 5000 mA g^{-1}, the power density increases from 142 W kg^{-1} to 8410 W kg^{-1} (see Supporting Information, Figure S5). Compared to supercapacitors, which addresses the extremes of power density

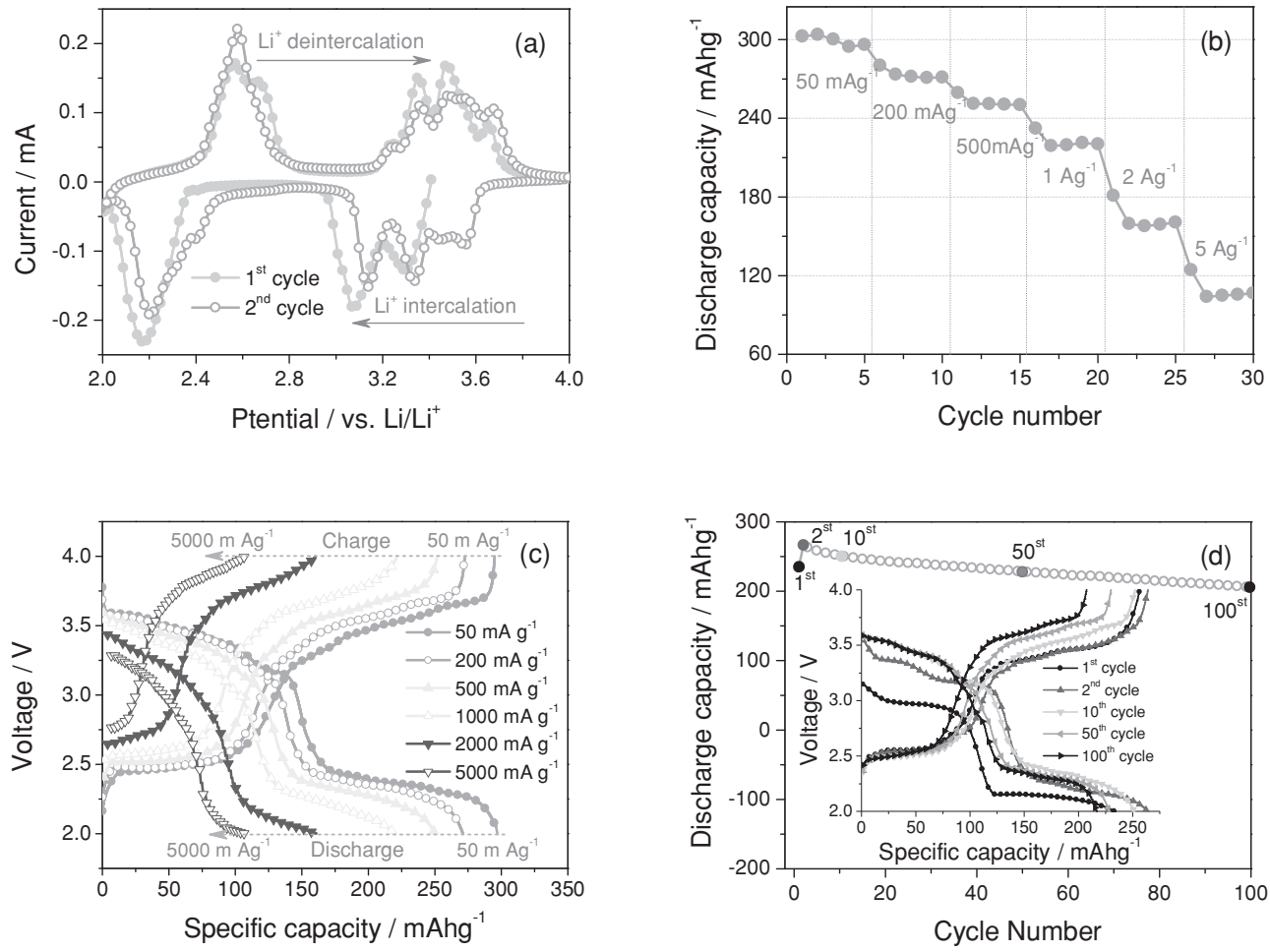

Figure 4. (a) CV curves of the first two cycles for leaf-like V_2O_5 nanosheets electrode at a scan rate of 0.2 mV s^{-1}. (b) Discharge capacities of leaf-like V_2O_5 nanosheets electrode at various current densities. (c) Charge/discharge curves of leaf-like V_2O_5 nanosheets electrode at various current densities. (d) Cycling performance of leaf-like V_2O_5 nanosheets electrode at a current density of 500 mA g^{-1}. Inset shows the charge/discharge curves correspond to different cycles.

needs (~1000–20000 W kg^{-1}) of commercially available devices, their energy density is only about 1–20 Wh kg^{-1}, the 2D leaf-like V_2O_5 nanosheets may be used for superior electrochemical energy-storage devices with both high-power density and high-energy density. Figure 4c presents the charge/discharge curves of the 2D leaf-like V_2O_5 nanosheets electrode at various current densities in the voltage window of 2.0–4.0 V. Good reversible plateau regions can be observed at all the current densities. The discharge/charge plateaus agree well with the redox peaks shown in the CV curve (Figure 4a). With the increase of current density, especially at very high current densities (2000 and 5000 mA g^{-1}), the discharge voltage decreases and the charge voltage increases due to the increasing polarization effect. Figure 4d shows the cycling performance of the 2D leaf-like V_2O_5 nanosheets electrode at a current density of 500 mA g^{-1}. After 100 cycles, the specific discharge capacity can be retained 206 mAh g^{-1}. The capacity fading rate is about 0.22% per cycle, which is lower than the results reported for this material.[5,19,21,26–29] The 2D leaf-like V_2O_5 nanosheets electrode maintains a well defined good reversible plateau region even at the 60th cycle. It is noticeable that the capacity loss with the plateau of about 3.15 V is much larger than those of others. Therefore, it can be inferred that the 2D leaf-like V_2O_5 processes relatively poorer reversibility for Li intercalation/deintercalation with the voltage plateau of about 3.15 V, which is considered a main reason for capacity fading. The excellent high rate performance of 2D leaf-like V_2O_5 nanosheets is believed to be based on their unique architecture results from the following aspect: The large specific area of the 2D leaf-like V_2O_5 nanosheets facilitates the electrolyte to transport the intercalation and deintercalation of the lithium ions; the hierarchical porous structure of the 2D leaf-like V_2O_5 nanosheets could effectively relax the mechanical strain generated upon the charge/discharge cycling.

Figure 5a gives the Nyquist plots of the 2D leaf-like V_2O_5 nanosheets electrode at various depth of discharge (DOD) after the electrode was activated at 20 mA g^{-1} for 4 cycles. The semicircle at the high frequency region relates to the combined process of surface film (R_{sf}) and the charge transfer resistance (R_{ct}). The low frequency semicircle (for 76%, 90%, and 100%

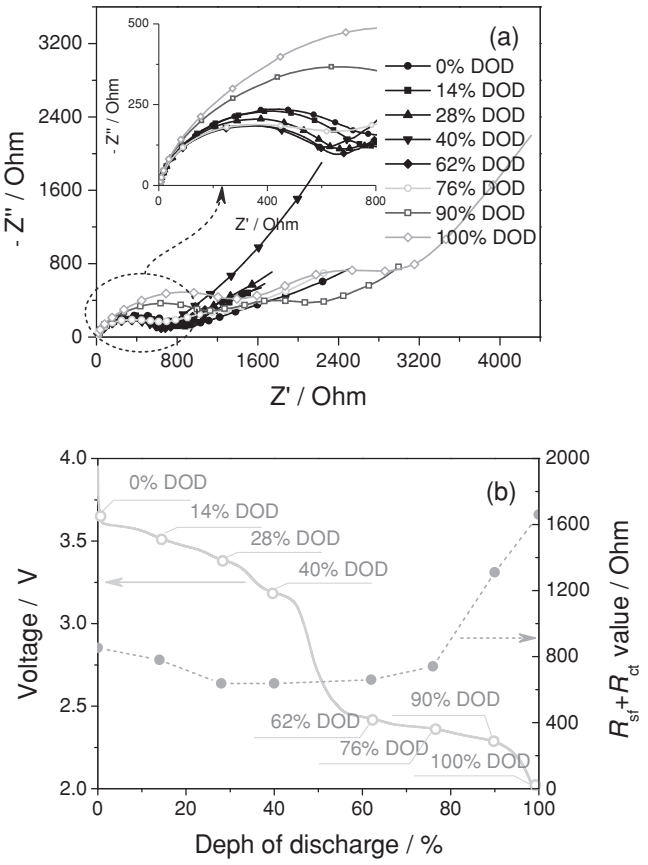

Figure 5. (a) Nyquist plots of leaf-like V_2O_5 nanosheets electrode measured at various depths of discharge (DOD). (b) The calculated $R_{sf+}R_{ct}$ values at the different depth of discharge state.

DOD) corresponds to the bulk phenomena, which arises from electronic conductivity of active material and ionic conductivity of the electrolyte filled in the pores of composite electrode.[30,31] Figure 5b presents the calculated R_{sf+ct} values (diameter of semicircle at high frequency) under various DOD states. With DOD increasing from 0% to 62%, the R_{sf+ct} value initially decreases from 853 Ω to 637 Ω at 28% DOD and then slightly increases to 660 Ω at 62% DOD. Further increasing DOD from 76% to 100% leads the R_{sf+ct} value abruptly increases from 740 Ω to 1660 Ω. Such a big increase of R_{sf+ct} value suggests that the electrochemical reaction under high DOD becomes much more difficult than under low DOD due to the change of phase structure. Another important feature of the EIS plots is the appearance of bulk resistance (R_b, the second semicircle at low frequency, see Supporting Information, Figure S6) under high DOD (76%, 90%, and 100% DOD) states. This suggests that under those states the electrode is a poor electronic conductor. While under low DOD (from 0% DOD to 62% DOD) states, the bulk resistance (R_b) is negligibly small, indicating that electrodes are good electronic conductors. This result is in good agreement with the four-probe current-voltage characteristics for $Li_xV_2O_5$ nanoribbons reported by Cui et al.[4] Large changes in R_b values have also been observed in some other cathode materials,[30–34] depending on the DOD, and are attributed to reversible semiconductor-metal transformations during cycling.

In summary, we have developed a facile, green, and low-cost synthesis of 2D leaf-like V_2O_5 nanosheets. The unique nanoscale characteristics, including 2D morphology, hierarchical porous structure, large specific surface, of these 2D V_2O_5 nanosheets leads to the superior electrochemical performance in terms of their specific capacity, rate capability, and cyclability when they are used as a cathode material for LIBs. The obtained excellent performance opens up new opportunities in the development of high performance next-generation LIBs used for alternative energy and electric transportation. The proposed synthetic method may be easily extended to other layered materials which can be used in broad fields including catalysis and sensors.

Experimental Section

Material preparation: Vanadium pentoxide gel was prepared using the method reported by Frontenot et al..[35] In brief, V_2O_5 powders (99.8%, Alfa-AESAR) were added into de-ionized water and H_2O_2 (30 *wt.*% in H_2O, Sigma-Aldrich) to form a solution with a V_2O_5 concentration (C_V) of 0.3 M and $n(H_2O_2)$: n(V) of 8:1. The resulting solution was stirred for 15 min while kept in water bath at a room temperature and then sonicated for 15 min for the reactions. This solution was later diluted to C_V = 0.056 M and then sonicated for about 80 min until the solution turned into brownish red V_2O_5 gel. This gel was further dispersed and diluted to a C_V of 0.03 M, and stirred in de-ionized water until a homogenous red-colored, viscous solution was formed. This solution was pre-frozen in a freeze refrigerator at −20 °C for 1 day and then freeze-dried under vacuum at −50 °C for 2 days in a Labconco FreeZone 1 L freeze dryer. After drying, the V_2O_5 cryogel was annealed in ambient atmosphere at 450 °C for 1 h to form 2D leaf-like V_2O_5 nanosheets.

Material characterization: The phase structure and morphology of the as-prepared samples were characterized by X-ray diffraction (XRD, Philips 1820 X-ray diffractometer), field emission scanning electron microscopy (FESEM, JEOL, JSM-7000), and transmission electron microscopy (TEM, Tecnai G2 F20 S-Twin). The Brunauer-Emmett-Teller (BET) specific surface areas and pore size distributions were measured with QuantaChrome NOVA 4200e analyzer (working gas N_2, 77 K).

Electrochemical measurements: The electrochemical properties of the 2D leaf-like V_2O_5 nanosheets were tested in coin-cells with metallic lithium as the anode and polypropylene (PP) film as separator. The coin-cells were assembled in an argon-filled glove-box. The cathodes were fabricated by mixing V_2O_5 nanosheets, super P carbon black, and poly(vinyldifluoride) (PVDF) at a weight ratio of 70: 20: 10 in *n*-methyl-2-pyrrolidone (NMP) solvent. The resulting mixture was then uniformly spread on an aluminum foil current collector. Finally, the electrode was dried at 80°C for 12 h. The electrode loading was about 2 mg cm^{-2} The electrolyte solution was made of 1 M $LiPF_6$ in a 1:1 (V:V) mixture of ethylene carbonate (EC) and dimethyl carbonate (DMC). The cells were galvanostatically charged and discharged under different current densities between 2.0 V and 4.0 V (*vs* Li/Li^+) using Arbin BT-2000 battery tester at room temperature. Cyclic voltammetry (CV) studies were carried out on an electrochemical workstation (CHI 605 C) between 2.0 and 4.0 V at a scan rate of 0.2 mV s^{-1}. Electrochemical impedance spectroscopies (EIS) were performed using the Solartron 1287A in conjunction with a Solartron 1260FRA/impedance analyzer. In EIS measurement, the frequency ranged from 100 kHz to 10 mHz and the AC amplitude was 5.0 mV.

Supporting Information

Supporting Information is available from the Wiley Online Library or from the author.

Acknowledgements

This research work has been financially supported in part by the National Science Foundation of the U.S. (CMMI-1030048), University of Washington TGIF, National Natural Science Foundation of China (51204061 and 21263003), and Guangxi Natural Science Foundation of China (2012jjAA20053).

Received: February 20, 2013
Published online: May 17, 2013

[1] M. Armand, J.-M. Tarascon, *Nature* **2008**, *451*, 652.
[2] T.-H. Kim, J.-S. Park, S. K. Chang, S. Choi, J. H. Ryu, H.-K. Song, *Adv. Energy Mater.* **2012**, *2*, 860.
[3] N.-S. Choi, Z. Chen, S. A. Freunberger, X. Ji, Y.-K. Sun, K. Amine, G. Yushin, L. F. Nazar, J. Cho, P. G. Bruce, *Angew. Chem. Int. Ed.* **2012**, *51*, 9994.
[4] C. K. Chan, H. L. Peng, R. D. Twesten, K. Jarausch, X. F. Zhang, Y. Cui, *Nano. Lett.* **2007**, *7*, 490.
[5] J. Liu, H. Xia, D. Xue, L. Lu, *J. Am. Chem. Soc.* **2009**, *131*, 12 086.
[6] J. Yan, A. Sumboja, E. Khoo, P. S. Lee, *Adv. Mater.* **2011**, *23*, 746.
[7] A. Pan, J.-G. Zhang, Z. Nie, G. Cao, B. W. Arey, G. Li, S.-Q. Liang, J. Liu, *J. Mater. Chem.* **2010**, *20*, 9193.
[8] M. S. Whittingham, *Chem. Rev.* **2004**, *104*, 4271.
[9] J. X. Wang, C. J. Curtis, D. L. Schulz, J. G. Zhang, *J. Electrochem. Soc.* **2004**, *151*, A1.
[10] R. Baddour-Hadjean, J. P. Pereira-Ramos, C. Navone, M. Smirnov, *Chem. Mater.* **2008**, *20*, 1916.
[11] Y. Wang, K. Takahashi, K. Lee, G. Cao, *Adv. Funct. Mater.* **2006**, *16*, 1133.
[12] P. G. Bruce, B. Scrosati, J.-M. Tarascon, *Angew. Chem. Int. Ed.* **2008**, *47*, 2930.
[13] J. Liu, X.-W. Liu, *Adv. Mater.* **2012**, *24*, 4097.
[14] J. Liu, J. S. Chen, X. Wei, X. W. Lou, X.-W. Liu, *Adv. Mater.* **2011**, *23*, 998.
[15] Y. Y. Liu, M. Clark, Q. F. Zhang, D. M. Yu, D. W. Liu, J. Liu, G. Z. Cao, *Adv. Energy Mater.* **2011**, *1*, 194.
[16] L. Mai, L. Xu, C. Han, X. Xu, Y. Luo, S. Zhao, Y. Zhao, *Nano Lett.* **2010**, *10*, 4750.
[17] A. M. Cao, J. S. Hu, H. P. Liang, L. J. Wan, *Angew. Chem. Int. Ed.* **2005**, *44*, 4391.
[18] Y.-S. Hu, X. Liu, J.-O. Muller, R. Schlogl, J. Maier, D. S. Su, *Angew. Chem. Int. Ed.* **2009**, *48*, 210.
[19] S. Wang, S. Li, Y. Sun, X. Feng, C. Chen, *Energy Environ. Sci.* **2011**, *4*, 2854.
[20] Q. Qu, Y. Zhu, X. Gao, Y. Wu, *Adv. Energy Mater.* **2012**, *2*, 950.
[21] Z. Wang, D. Xu, L. Wang, X. Zhang, *ChemPlusChem* **2012**, *77*, 124.
[22] V. Petkov, P. N. Trikalitis, E. S. Bozin, S. J. L. Billinge, T. Vogt, M. G. Kanatzidis, *J. Am. Chem. Soc.* **2002**, *124*, 10157.
[23] J. Livage, *Chem. Mater.* **1991**, *3*, 578.
[24] C. Delmas, H. Cognac-Auradou, J. M. Cocciantelli, M. Ménétrier, J. P. Doumerc, *Solid State Ionics* **1994**, *69*, 257.
[25] R. Baddour-Hadjean, A. Marzouk, J. P. Pereira-Ramos, *J. Raman Spectrosc.* **2012**, *43*, 153.
[26] A. Sakunthala, M. V. Reddy, S. Selvasekarapandian, B. V. R. Chowdari, P. Christopher Selvin, *Energy Environ. Sci.* **2011**, *4*, 1712.
[27] J. Liu, Y. Zhou, J. Wang, Y. Pan, D. Xue, *Chem. Commun.* **2011**, *47*, 10380.
[28] S. Wang, Z. Lu, D. Wang, C. Li, C. Chen, Y. Yin, *J. Mater. Chem.* **2011**, *21*, 6365.
[29] Y. Wang, H. J. Zhang, K. W. Siah, C. C. Wong, J. Lin, A. Borgna, *J. Mater. Chem.* **2011**, *21*, 10336.
[30] M. V. Reddy, G. V. Subba Rao, B. V. R. Chowdari, *J. Phys. Chem. C* **2007**, *111*, 11712.
[31] M. D. Levi, D. Aurbach, *J. Phys. Chem. B* **2004**, *108*, 11693.
[32] M. V. Reddy, S. Madhavi, G. V. Subba Rao, B. V. R. Chowdari, *J. Power Sources* **2006**, *162*, 1312.
[33] D. Aurbach, M. D. Levi, E. Levi, H. Teller, B. Markovsky, G. Salitra, U. Heider, L. Heider, *J. Electrochem. Soc.* **1998**, *145*, 3024.
[34] F. Nobili, F. Croce, B. Scrosati, R. Marassi, *Chem. Mater.* **2001**, *13*, 1642.
[35] C. J. Fontenot, J. W. Wiench, M. Pruski, G. L. Schrader, *J. Phys. Chem. B* **2000**, *104*, 11622.